Smart Structures and Systems, *Vol. 15, No. 2 (2015) 335-353*
DOI: http://dx.doi.org/10.12989/sss.2015.15.2.335

Issues in structural health monitoring for fixed-type offshore structures under harsh tidal environments

Byung-Jin Jung[1,2a], Jong-Woong Park[3b], Sung-Han Sim[4c] and Jin-Hak Yi[*1,2]

[1]*Coastal and Environmental Engineering Division, Korea Institute of Ocean Science and Technology, 787 Haean-ro, Sangrok-gu, Ansan, Republic of Korea*
[2]*Department of Convergence Study on the Ocean Science and Technology, Ocean Science and Technology School, Korea Maritime and Ocean University, 727 Taejong-ro, Yeongdo-gu, Busan, Republic of Korea*
[3]*Department of Civil and Environmental Engineering, University of Illinois at Urbana-Champaign, 205 North Mathews Ave., Urbana, Illinois, USA*
[4]*School of Urban and Environmental Engineering, Ulsan National Institute of Science and Technology, 50 UNIST-gil, Ulju-gun, Ulsan, Republic of Korea*

(Received December 30, 2014, Revised January 19, 2015, Accepted January 20, 2015)

Abstract. Previous long-term measurements of the Uldolmok tidal current power plant showed that the structure's natural frequencies fluctuate with a constant cycle—i.e., twice a day with changes in tidal height and tidal current velocity. This study aims to improve structural health monitoring (SHM) techniques for offshore structures under a harsh tidal environment like the Uldolmok Strait. In this study, lab-scale experiments on a simplified offshore structure as a lab-scale test structure were conducted in a circulating water channel to thoroughly investigate the causes of fluctuation of the natural frequencies and to validate the displacement estimation method using multimetric data fusion. To this end, the numerical study was additionally carried out on the simplified offshore structure with damage scenarios, and the corresponding change in the natural frequency was analyzed to support the experimental results. In conclusion, (1) the damage that occurred at the foundation resulted in a more significant change in natural frequencies compared with the effect of added mass; moreover, the structural system became nonlinear when the damage was severe; (2) the proposed damage index was able to indicate an approximate level of damage and the nonlinearity of the lab-scale test structure; (3) displacement estimation using data fusion was valid compared with the reference displacement using the vision-based method.

Keywords: structural health monitoring (SHM); added mass; nonlinearity; damage detection; displacement estimation; tidal current power plant structure

1. Introduction

With increasing interest in renewable energy, studies on ocean energy, such as tidal and wave energy, have been actively conducted. The Uldolmok tidal current power plant (TCPP) was built in

*Corresponding author, Ph.D., Principal Research Scientist, E-mail: yijh@kiost.ac
[a] Graduate Student, E-mail: bjung@kiost.ac
[b] Ph.D., Post-Doctoral researcher E-mail: jongwoon@illinois.edu
[c] Ph.D., Assistant Professor, E-mail: ssim@unist.ac.kr

http://www.techno-press.org/?journal=sss&subpage=8 ISSN: 1738-1584 (Print), 1738-1991 (Online)

2009 near the Jindo Grand Bridge to develop technologies for tidal current power generation and to prepare for widespread implementation. Its performance in terms of the grid connection and power efficiency was verified (Han *et al*. 2013). The structure experienced difficulties during construction because the tidal current on the Uldolmok Strait has very high speeds of up to 4–5 m/s and a short tidal stand time of approximately 30 min. Therefore, there had been various attempts to maintain structural stability in this severe environment, including installing temporary loading blocks and mooring the plant with mooring chains. Also, the strain responses were measured and dynamic characteristics were monitored in the long term to secure stability in construction and maintain it effectively during operation (Yi *et al*. 2012). The Uldolmok TCPP's natural frequencies—one of its important dynamic characteristics—was found to fluctuate in the same period as the tidal cycle—i.e., approximately 6 hours and 12 hours, which are the periods of M4 and M2 tidal constituents, respectively. In addition, it was necessary to determine the cause of this; the first natural frequency fluctuated and varied by up to 16% in a day, which is relatively much greater than that of onshore structures, including buildings and bridges (Yi *et al.* 2013b). This observation was the motivation behind this study. The first frequency, tidal current velocity, and tidal height of the Uldolmok TCPP are shown in Fig. 1.

The natural frequency is a typical damage factor and its change is closely related to structural damage in terms of SHM (Salawu 1997, Kim and Stubbs 1995). Therefore, it is important to find the reason why the Uldolmok TCPP's first natural frequency has fluctuated. Also, many studies have been carried out to estimate the damage of infrastructures using untypical methods such as modal strain energy (Huynh *et al*. 2013).

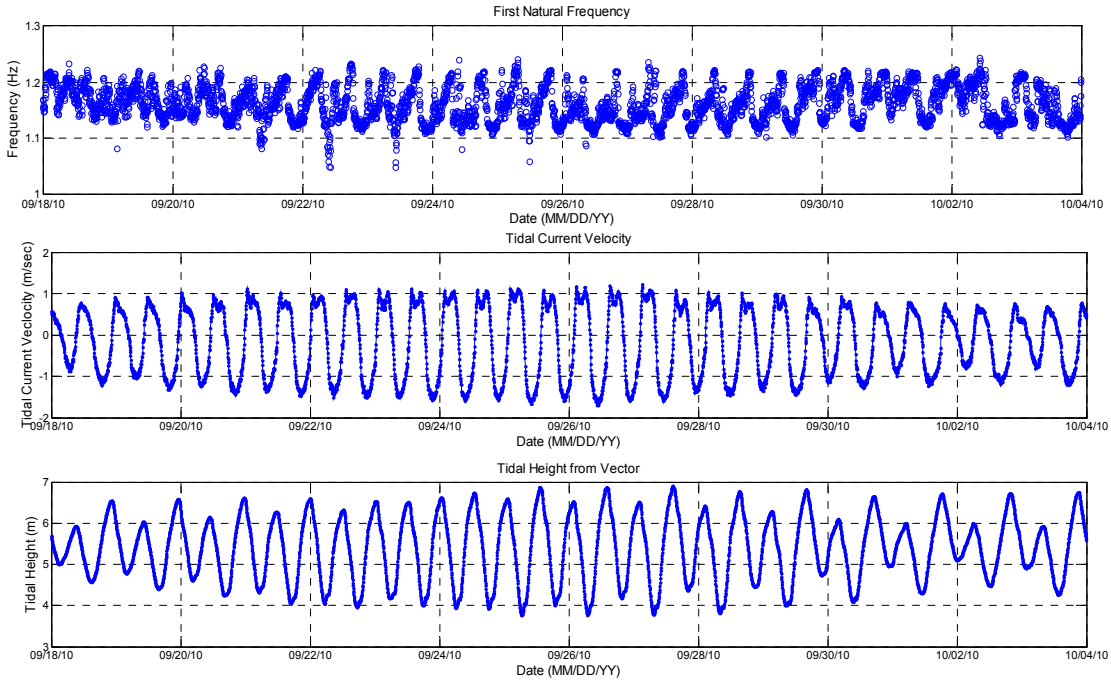

Fig. 1 The first natural frequency and tidal changes of the Uldolmok tidal current power plant from September 18 to October 3, 2010 (Yi *et al*. 2013b)

Displacement can also be a vital damage index (Li *et al.* 2014). Monitoring displacement helps us to intuitively and directly realize structure conditions, such as detecting structural damage and deformation, from the external loads. Measuring displacement is possible with the use of several methods, including a linear variable differential transformer (LVDT), a LASER Doppler Vibrometer (LDV) (Nassif *et al*. 2005), a global positioning system (GPS) (Celibi 2000), and a vision-based displacement meter. However, these methods are not usually appropriate for offshore structures. Using an LVDT in offshore structures is impossible; it needs a fixed point to measure relative displacement. An LDV has high resolution and performance, however it is very costly. As for GPS, the resolution is too low to suitably measure displacement. A vision-based displacement meter is sensitive to weather and is limited in field applications. However, a strain gauge and accelerometer are easy to install on the structure and obtain strain and acceleration responses. Indirect displacement can be estimated economically by fusing the strain and acceleration responses. Park *et al*. (2013) proposed the data fusion method using strain and acceleration responses and validated this method by comparing the estimated displacement from data fusion to the measured displacement from a LASER displacement sensor through the field experiments on the Sorok Bridge. Cho *et al*. (2014) numerically validated various types of beam structures using this method. It is necessary to conduct experiments to validate this data fusion method in cantilever beams such as those used in the monopole-type tidal turbines like MCTs (Marine Current Turbines) (Fraenkel 2007).

This study investigates the important issues in SHM systems for offshore structures that are generally exposed to a harsh environment with strong tidal forces. The critical issues discussed in this study include:

- Identification of dynamic behavior under the tidal current
- Damage detection tailored to offshore structures
- Displacement-based structural condition assessment

These issues are experimentally examined using a scale model in a circulating water channel. A finite element (FE) model of the lab-scale test structure is built using ABAQUS to support the experimental results.

2. Theoretical backgrounds

2.1 Added mass

A tubular lab-scale test structure was used in this experiment because many offshore structures, including the Uldolmok TCPP, consist of this kind of section. Where the Keulegan-Carpenter number (K_c) is less than 3, the added mass (M_a) can be written as Eq. (1) in the case of the cylindrical section (DNV 2010).

$$M_a = \rho \pi a^2 \tag{1}$$

where ρ and a are the density of fluid and radius of the cylinder section, respectively. When a structure is affected by added mass, the i-th natural frequency can be calculated as Eq. (2).

$$f_i = \frac{1}{2\pi}\sqrt{\frac{K_i}{M_i + M_{ai}}} \tag{2}$$

where M_i, K_i , and M_{ai} are the generalized mass ($\phi_i^T M \phi_i$), stiffness ($\phi_i^T M \phi_i$), and added mass ($\phi_i^T M_a \phi_i$) of the i-th mode, respectively, where ϕ_i, M, and K are the mode shape matrix of the i-th mode, mass matrix, and stiffness matrix of a structure, respectively. Added mass can be influenced by the relative velocity between fluid and a structure, period of the structure, and surface roughness in a case where $K_c$is larger than 3. Therefore, the added mass shown in Eq. (1) can be considered as a simplified form for the practical design purposes.

2.2 Displacement estimation using data fusion

Lee *et al*. (2010) proposed an FIR (finite impulse response) filter using acceleration to estimate displacement. The estimated displacement, u ,can be calculated as Eq. (4) using the measured acceleration, $\overline{a}$, with a sampling time step, Δt , which is the analytical solution of Eq. (3) known as the Tikhonov regularization scheme.

$$\underset{u}{\text{Min}}\,\Pi = \frac{1}{2}\left\| L_a \left(L_c u - (\Delta t)^2 \overline{a} \right) \right\|_2^2 + \frac{\lambda^2}{2}\|u\|_2^2 \tag{3}$$

$$u = (L^T L + \lambda^2 I)^{-1} L^T L_a \overline{a} (\Delta t)^2 = C_a \overline{a} (\Delta t)^2 \tag{4}$$

where L_a and L_c are a diagonal weighting and a linear algebraic operator matrices, the superscript T denotes the matrix transpose, $\|\bullet\|_2$ is the two-norm of a vactor; and λ is the optimal regularization factor, which is determined by the number of data points during the first natural period. Detailed information on derivation can be found in Lee *et al*. (2010). This method is limited in estimating quasi-static displacement. Park *et al*. (2013) developed this method by adding the quasi-static displacement component from the strain response, $\overline{\varepsilon}$,—the so-called data fusion in Eqs. (5) and (6).

$$\underset{u}{\text{Min}}\,\Pi = \frac{1}{2}\left\| L_a (L_c u - (\Delta t)^2 \overline{a}) \right\|_2^2 + \frac{\lambda^2}{2}\|u - D\{\overline{\varepsilon}\}\|_2^2 \tag{5}$$

$$u = (L^T L + \lambda^2 I)^{-1}(L^T L_a \overline{a} \Delta t^2 + \lambda^2 \alpha D \overline{\varepsilon}) = \begin{bmatrix} C_a \Delta t^2 & C_\varepsilon \end{bmatrix} \begin{bmatrix} a \\ \overline{\varepsilon} \end{bmatrix} = C_a a (\Delta t)^2 + C_\varepsilon \overline{\varepsilon} \tag{6}$$

where $L=L_aL_c$, $C_a = (L^T L + \lambda^2 I)^{-1} L^T L_a$, D is the strain-displacement transformation matrix, and $\alpha$is the scaling factor of strain-displacement relationship (Park *et al*. 2013)

2.3 Damage index (β)

The displacement and strain responses in the finite number of modes $\{u\}_{m\times 1}$ and $\{\varepsilon\}_{n\times 1}$ can be formulated by Eqs. (7) and (8).

$$\{u\}_{m\times 1} = \Phi_{m\times r}\ \{q\}_{r\times 1} \tag{7}$$

$$\{\varepsilon\}_{n\times 1} = \Psi_{n\times r}\ \{q\}_{r\times 1} \tag{8}$$

where $\Phi_{m\times r}$ and $\Psi_{n\times r}$ are the displacement and strain mode shape matrices, respectively; $\{q\}_{r\times 1}$ is the modal coordinate; m and n are the number of measurements; and r is the number of selected modes. In $n \geq r$, eliminating $\{q\}_{r\times 1}$ from Eqs. (7) and (8) yields Eq. (9).

$$\{u\}_{m\times 1} = \Phi_{m\times r}\ \Psi^{+}_{n\times r}\{\varepsilon\}_{n\times 1} \tag{9}$$

Dynamic displacement and quasi-static displacement can be theoretically obtained from Eq. (4) and Eq. (9), respectively. Estimation of dynamic displacement is quite accurate. However, it is hard to estimate quasi-static displacement; since, the neutral axis of a structure can depend on the load intensity when the structure does not have perfect symmetric structural property. We introduced the term α in order to solve this problem.

$$\alpha = \sqrt{\frac{S_{d,acc}(f_1)}{S_{d,strain}(f_1)}} \tag{10}$$

where α is a scaling coefficient and has a ratio of $S_{d,acc}(f_1)$ to $S_{d,strain}(f_1)$. $S_{d,acc}$ and $S_{d,strain}$ are the power spectral densities of the displacement from acceleration and strain, respectively; and f_1 denotes the first natural frequency. By multiplying Eqs. (9) and (10), quasi-static displacement can be also obtained accurately as Eq. (11)

$$\{u\}_{m\times 1} = \alpha_{m\times m}\ \Phi_{m\times r}\ \Psi^{+}_{n\times r}\{\varepsilon\}_{n\times 1} \tag{11}$$

In addition, the term α only relies on the modal property and it has a particular value in an Intact Case; however, the presence of structural damage causes this coefficient to change. Therefore, α in Eq. (10) can be defined as the damage index. Eq. (12) shows damage index, which has the same base as the normalized damage factor (NDF) proposed by Park *et al*. (2014).

$$\beta = \left\{ \frac{\alpha_{Damage\ case}}{\alpha_{Intact\ case}} - 1 \right\} \times 100 \tag{12}$$

where $\alpha_{Intact\ Case}$, $\alpha_{Damage\ Case}$ are the scaling coefficients in Intact Case and Damage Case, respectively.

3. Experimental study using circulating water channel

3.1 General information on the lab-scale experiments

Changes in the natural frequencies are related to the mass and stiffness of structures, and they are directly connected to structural integrity; therefore, it is very important to study the cause of these changes. First, it is necessary to analyze the effect of added mass because the change of mass influences the structural system. When submerged or semi-submerged structures are vibrated in fluid, the fluid mass of the submerged portion of a structure is added to its self-weight. As a result, the natural frequency decreases and the modal damping ratio increases compared to when it is not submerged (Weiner *et al*. 1994, Sedlar *et al*. 2011, Lee *et al.* 2012, Lee *et al.* 2013). Second, temperature changes and local damages in structures can affect the stiffness of the structure and can also affect the natural frequency. Temperature changes were not considered in this lab-scale

experiment on the basis of the fact that the fluctuation in the temperature of the sea—from approximately 1 to 2°C per day around the Uldolmok TCPP—did not greatly influence the natural frequencies. In addition, there could be difficulties with the grouting operations connecting the jacket support-structure and its foundation; even if these operations were successfully carried out, the concrete grout would be cracked by the fatigue. Cracks can cause nonlinearity in a structure. Even if the natural frequencies are independent of the applied force, we needed to examine the dynamic response with an increasing current velocity, which is the governing load for the Uldolmok TCPP. The lab-scale experiments to find the main factor that influences the natural frequencies were performed by considering that the dependent variables of the natural frequencies change as the water level changes and that the boundary damages change between the support structure and its foundation with increasing current velocity.

To verify the proposed method to estimate displacement, we needed random excitation to simulate natural conditions and to make not only dynamic displacement but also quasi-static displacement. The current can generate dynamic displacement. Quasi-static displacement was induced to maintain the current velocity. The current velocity was controlled by adjusting the valve controlling the water quantity and the sluice gate located at the end of a circulating water channel.

Therefore, three different lab-scale experiments were performed:

1. To investigate the effect of added mass on the lab-scale test structure by controlling the water level without flow;
2. To investigate how the damage levels of the lab-scale test structure affect its natural frequencies under different load conditions—i.e., by increasing the current velocity; and
3. To verify the proposed displacement estimation method by increasing, maintaining, and decreasing the current velocity.

3.2 Information on the lab-scale test structure

The lab-scale experiments were conducted in a circulation water channel, as shown in Fig. 2. The circulating water channel can generate the water current uniformly and control the water level. Note that the structural behaviors of the Uldolmok TCPP have been influenced more by the tidal current than by waves.

The lab-scale test structure of the Uldolmok TCPP was designed in the shape of a monopile support structure. The natural frequencies of the test structure are higher than those of the Uldolmok TCPP—unlike the original intention—because of the use of the commercially available steel pipe and the limitations in a pipe height. In general, Reynolds similarity rule can be used to evaluate the flow-induced lift force and other related works. Meanwhile Froude similarity rule can be applied to evaluate the wave forces on a coastal structure, such as caissons and blocks of breakwater, which are subjected to waves (Yi *et al*. 2013a). However, these similarity rules were not used in this lab-scale experiment; since this is beyond the scope of this study. The objective of this study is limited to analyze the effect of added mass and the stiffness of the foundation on the structural dynamic characteristics. Additional research on the Strouhal number should be conducted to analyze the vortex frequency. As shown in Fig. 3, the lab-scale test structure is made of stainless steel, and its height, diameter, and thickness are 1.1 m, 38 mm, and 2 mm, respectively.

As shown in Fig. 4, accelerometers were installed on the top plate to measure acceleration in the fore-and-aft and side-to-side directions, and two accelerometers in the fore-and-aft direction were used to obtain not only bending modes but also the torsional modes. The selected accelerometers are integrated circuit piezoelectric(ICP) Type 355B53, PCB Piezotronics, Inc.

Strain gauges were installed on the column at 100mm from the bottom. Strain gauge Wheatstone bridges were configured with a half-bridge—two for measuring in the fore-and-aft direction and two for measuring in the side-to-side direction. Temperature effect was ignored in the lab-scale experiment. Waterproof material was attached to prevent distortion of the strain response. The accelerometers and strain responses were obtained with a sampling rate of 300 Hz by MGCPlus (HBM 2014), a data acquisition device (DAQ) produced by HBM, Inc. The real displacement was measured by recording the target on the top-plate using a camcorder. Although there are many methods to measure real displacements, it was difficult to affix this to the channel. The pump of the circulating water channel generated vibration on the experimental field, and there was much more vibration on the channel due to flow. This is why we could not install a LASER displacement meter on the channel to measure structural behavior in the current direction and used a camcorder instead to measure them from the outside of the water channel. Because the camcorder records at 30 frames per second (fps), the first bending modal frequency of the lab-scale test structure (8.59 Hz) could be detected. To reduce the error and to improve the accuracy, the camcorder was installed as closely as possible to the lab-scale test structure. An image processing technique was employed to extract the displacement from the recording data (Yi *et al*. 2013c). The hydrometer was installed at least 5 m from the front of the lab-scale test structure to avoid flow interference.

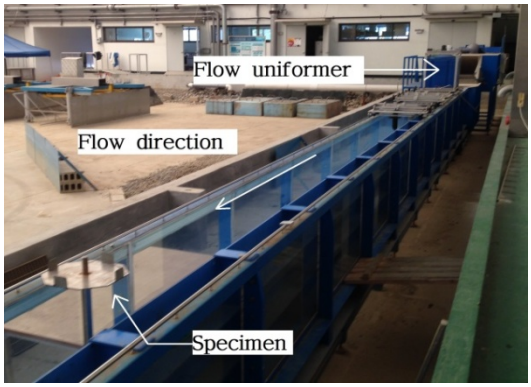

Fig. 2 Setup for the lab-scaleexperiment

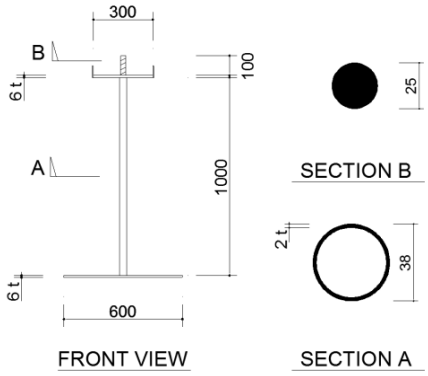

Fig. 3 Dimensions of the lab-scale test structure

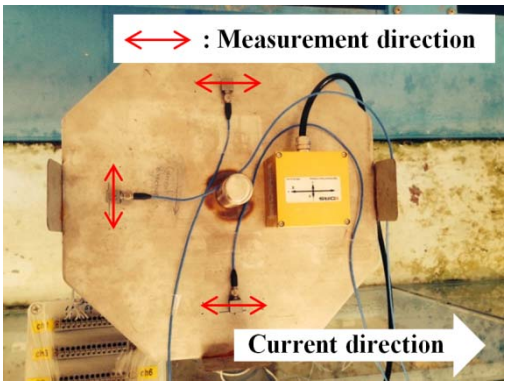

(a) Accelerometer location

(b) Strain gauge location

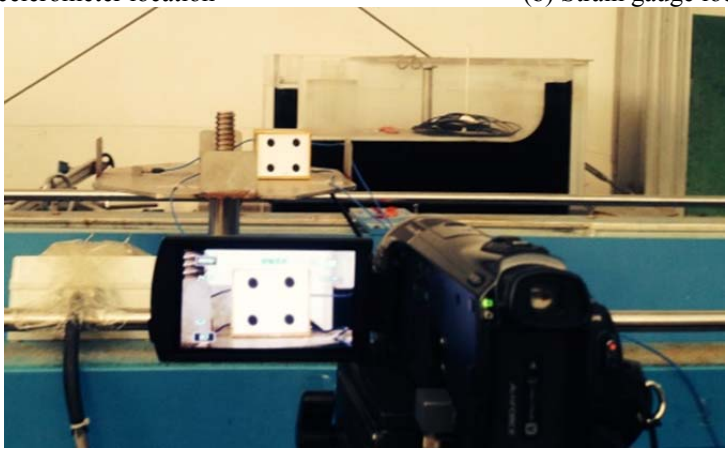

(c)Camcorder setup to measure real displacement

Fig. 4 Sensors and device used forthe lab-scale experiment

3.3 Outline of the lab-scale experiment

The first lab-scale experiment is to observe the natural frequency with various water levels. Table 1 lists the order of the first lab-scale experiment. In this experiment, the boundary condition is intact, which means that all bolts are fastened, as shown in Fig. 5. Tidal level changes on the Uldolmok Strait were simulated by water level changes in the circulating water channel. Changes in the water level can be changes of added mass. For this experiment, which was conducted without a current, the acceleration response was obtained from impact excitation. After the fast Fourier transform (FFT) analysis, the natural frequencies are obtained by reading the peak frequency—i.e., peak-peaking method— in the frequency domain (Yi *et al*. 2004). However, the FFT resolution is not high enough to observe the variation of the natural frequencies. The eigen system realization algorithm (ERA) method analyzed in the time domain was employed to allow more resolution in the frequency change compared with using FFT (Juang and Pappa 1985).

Table 1 Order of the first lab-scale experiment

Water level (mm)	Current velocity (m/s)	Boundary condition
From 0 to 800 at an interval of 100	0	Intact Case

The second experiment was performed with the changing current velocity and changing boundary connections, i.e., intact and two damage cases. As shown in Fig. 5, these three cases are (1) Intact case; (2) Damage Case 1; and (3) Damage Case 2. In Intact Case, the foundation of the lab-scale test structure and the bottom of the water channel are connected by fastening four bolts. Damage Case 1 is the condition with three fastened bolts, and Damage Case 2 is the condition with two fastened bolts which are set diagonally. The order of the second experiment is given in Table 2. Because the lab-scale test structure was subjected to the current load, which causes ambient vibration, extra excitation was not needed. The natural frequencies are obtained using the former method of the first experiment. The acceleration responses were recorded with a sampling rate of 300 Hz.

In the third lab-scale experiment, water was stored at a 350 mm level in the channel without flowing before the experiment began. After the pump started operation, the valve was opened gradually, maintaining at water level at 350 mm. The valve was released completely to generate maximum current velocity. After several seconds, the pump was turned off. Displacement of the lab-scale test structure was generated through such a method. We carried out the same experiments three times for the three boundary conditions.

Table 2 Order of the second lab-scale experiment

Water level (mm)	Current velocity (m/s)	Boundary condition
350	0.39, 0.65, 0.92, 1.14, 1.31	Intact Case (four bolts)
350	0.39, 0.65, 0.92, 1.14, 1.31	Damage Case 1 (three bolts)
350	0.39, 0.65, 0.92, 1.14, 1.31	Damage Case 2 (two bolts)

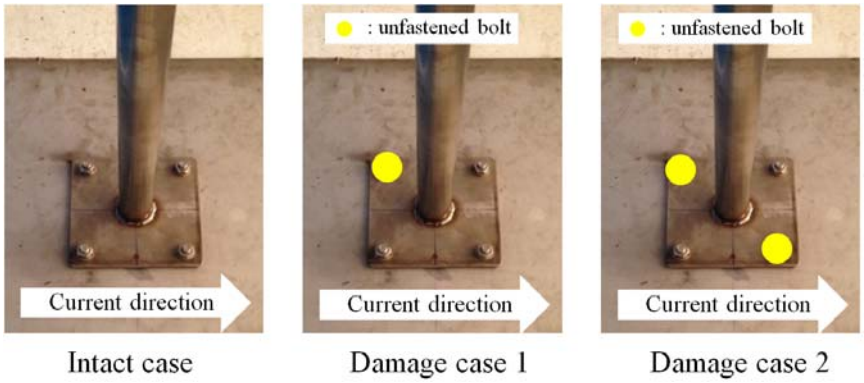

Fig. 5 Definition of boundary conditions between the lab-scale test structure and the bottom

3.4 Analysis of experimental results

3.4.1 Added mass effect

Fig. 6 shows the acceleration responses under impact excitation at a 500 mm water level, and Fig. 7 shows the results for the first lab-scale experiment—the first and second bending modes in the fore-and-aft and side-to-side directions. In the case of the first bending mode, theoretically, the natural frequency should decrease as the water level increases. However, the first natural frequency in the fore-and-aft direction increased from 8.59 to 8.61 Hz by 0.02 Hz from 0 to 400 mm for the water level, and that in the side-to-side direction also increased from 9.09 to 9.11 Hz by 0.02 Hz. More discussion or additional tests may be needed. For more than a 400mm water level, the natural frequencies for the first bending modes are, however, slightly reduced as the water level increases, but the change is very small—i.e., 0.58% from 8.61 to 8.56 Hz in the first modal frequency in the fore-and-aft direction and 0.76% from 9.11 to 9.04 Hz in the first modal frequency in the side-to-side direction. The second modal frequencies obviously decreased, as shown in Fig. 6(b) by 11.3%. This is a reasonable result because the lower part of the cantilever beam has more modal sensitivities in case the second mode shape, as shown in Fig. 8. The reason why there are differences between the first and second natural frequencies in the fore-and-aft direction from the side-to-side direction is due to asymmetry mass and stiffness of the lab-scale test structure. If structures have the perfect symmetry, the first and second natural frequencies would be the same.

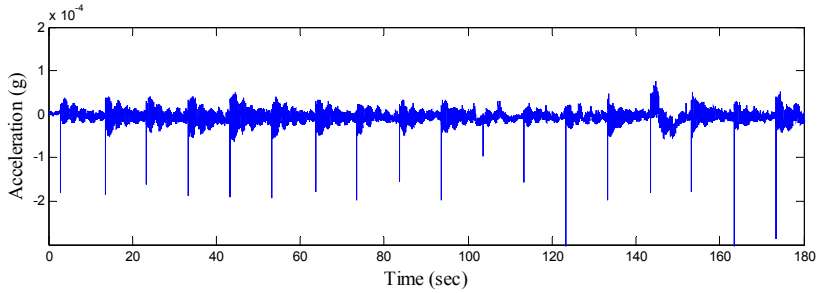

Fig. 6 Acceleration time history response by impact excitation (500mm water level, fore-and-aft direction).

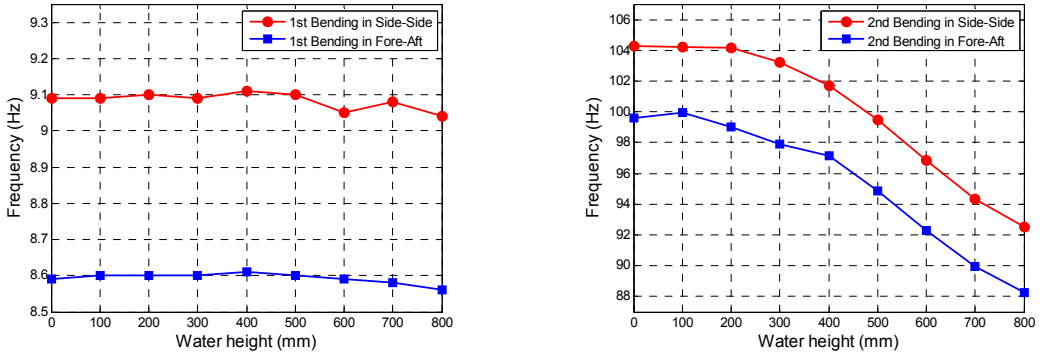

(a) First bending modes (b) Second bending modes

Fig. 7 Results of the first lab-scale experiment (added mass effect)

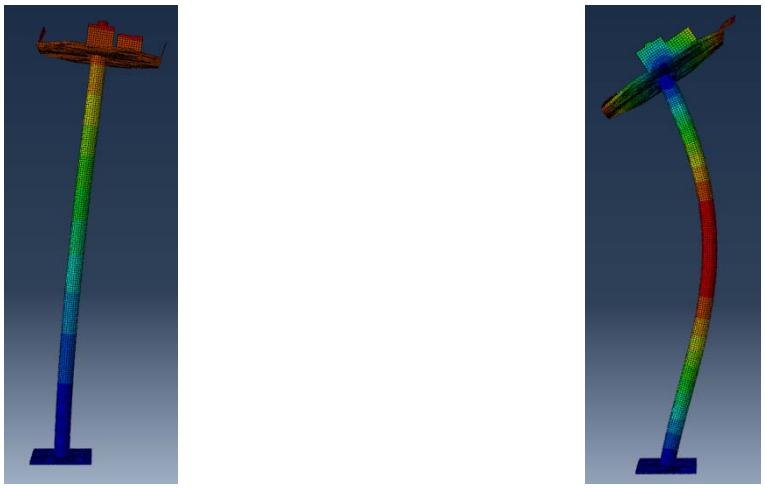

(a) First bending mode shape (8.59 Hz) (b) Second bending mode shape (99.73 Hz)

Fig. 8 First and second bending mode shapes of the lab-scale test structure's numerical model in dry condition

3.4.2 Boundary damage effect from current velocity change

Fig. 9 shows the result of the second experiment in Damage Case 2. Power spectral density (PSD) data from the acceleration responses in every current velocity in Damage Case 2 are plotted in Fig. 9(a). The amplitude increases as the current velocity increases. Fig. 9(b) shows a partial extension of the circle marker in Fig. 9(a); this indicates the first bending modal frequency in the fore-and-aft direction. The peak frequencies gradually decrease with the increasing current velocity. The first natural frequencies of all boundary conditions are summarized in Fig. 10. In the cases of the intact condition and Damage Case 1, there were slight changes in the natural frequencies; however, the first natural frequency in Damage Case 2 decreased from 7.3 to 6.7 Hz—up to 8.25% with increasing water velocity. The reason why the natural frequencies decrease as the degree of the damage of the boundary connections becomes severe is due to reduction of stiffness in the boundary connections. Also, no effects of water velocity in Intact Case and Damage Case 1 indicate that the whole system of the lab-scale test structure is a linear system. However, if the damage of the boundary connection is severe such as in Damage Case 2, decreasing the natural frequency as the water velocity increases means that the lab-scale test structure may behave as a nonlinear system. Because the condition of the boundary connection is only changed in this experiment, the boundary connection is nonlinear. Therefore, the damage at the foundation is much more influential than the effect of the added mass associated with the tidal height in that the first frequency of the Uldolmok TCPP varies up to 16% in a day, and severe damage at the foundation can cause nonlinearity in the structural system. Hence, it can be concluded that the natural frequency decreases more significantly as the damage at the foundation becomes severe. However, as for the stability of the whole structure, additional research is needed to evaluate quantitative damages.

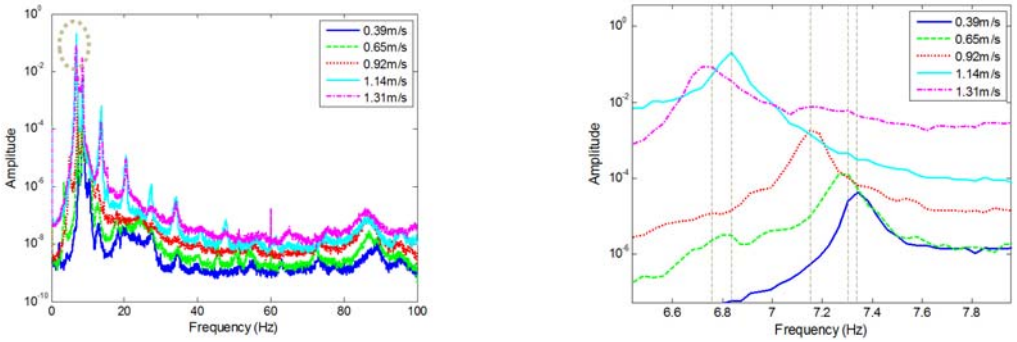

(a) PSD data from acceleration in Damage Case 2 (b)Specific change in the first natural frequency

Fig. 9 Result of the second lab-scale experiment in Damage Case 2 and its detail

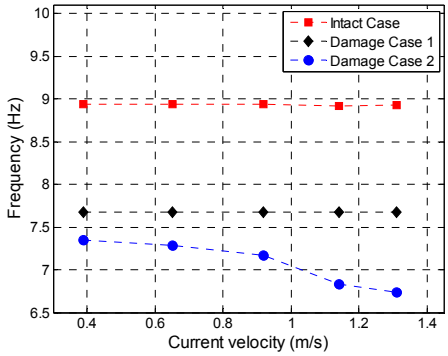

Fig. 10 Changes in the first natural frequency in Intact Case, Damage Case 1, and Damage Case 2 as current velocity increases

3.4.3 Damage index (β)

Traditionally, efforts to easily and accurately determine the level of structural damage have been made by many damage indexes, such as the natural frequency, modal shape, and modal curvature. The proposed damage index β in this study can be obtained by fusing data to estimate displacement, as shown in Eqs. (6), (11), and (12). Therefore, it is beneficial to detect the damage and estimate displacement simultaneously. The third lab-scale experiment to estimate displacement is carried out three times over three boundary conditions, and Fig. 11 shows each β value of Damage Cases 1 and 2. The damage index β in Damage Case 1 has a larger value than Damage Case 2; i.e., the boundary damage becomes severe. The damage index β in Damage Case 1 has almost the same value. On the other hand, there is a difference between the maximum and minimum values of β by 1.88 in Damage Case 2; it is a large amount compared to that of Damage Case 1, by 0.134, as shown in Table 3. If more cases of Damage Case 2 are conducted, it could be discerned whether the third β of Damage Case 2 can be ignored as an experimental error by statistical analysis. Regarding this experiment result in itself, if the damage index β is monitored, we could determine whether the damage is ongoing. A large difference in β may mean that the structural system of Damage Case 2 is nonlinear.

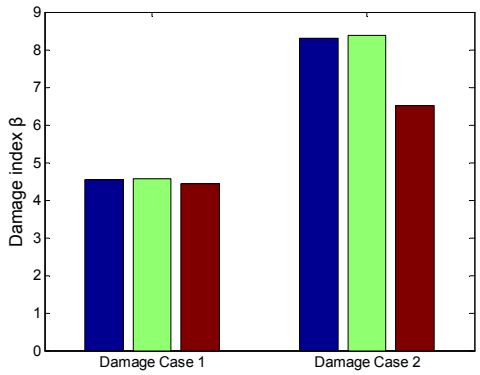

Fig. 11 Damage index β for Damage Case 1 and Damage Case 2

Table 3Difference between maximum and minimum of βfor Damage case 1 and Damage Case 2

Boundary condition	Intact Case	Damage Case 1	Damage Case 2
Difference between maximum and minimum of β	—	0.134	1.88

3.4.4 Displacement estimation

As shown in Fig. 12, the results of the third experiment are plotted by two of every boundary condition. The real displacement from image processing and the estimated displacement from data fusion have similar trends. The pump and valve could generate ambient vibration; the pump was turned off during this experiment, and the pump has a large capacity. It maintains maximum current velocity by 1.31 m/s in the circulating water channel with a width of 600 mm and a height of 350 mm. It is possible for this vibration to be transmitted to the camcorder on the tripod and introduce with experimental errors because the maximum displacement of the lab-scale test structure is very small—approximately 0.08 mm. In Fig. 12(b) in particular, it seems that the real displacement increased before the pump was turned off; however, this could be attributed to an experimental error (compared to the trends of other cases). We introduced two error factors, as shown in Eqs. (13) and (14): Err_1 is the deviation of the maximum real (vision-based) and estimated displacements ($u_{real,max}$ and $u_{estimated,max}$), and Err_2 is the root mean square error (RMSE) of the deviation between the real and the estimated displacements(u_{real} and $u_{estimated}$). The Err_1 and Err_2 values of all cases are listed in Table 4. The two values decrease as the damage becomes severe; in other words, errors can be reduced when displacement is larger.

$$Err_1 = \left| u_{real,\max} - u_{estimated,\max} \right| \tag{13}$$

$$Err_2 = \frac{RMSE\left(u_{real} - u_{estimated} \right)}{RMSE\left(u_{real} \right)} \tag{14}$$

Table 4 Err_1 and Err_2 of Intact Case, Damage Case 1, and Damage Case 2

Experimental cases	Intact Case		Damage Case 1		Damage Case 2	
	First try	Second try	First try	Second try	First try	Second try
Err_1	0.0151	0.0155	0.0083	0.0091	0.0068	0.0035
Err_2	0.4823	0.6113	0.2962	0.2608	0.2302	0.1029

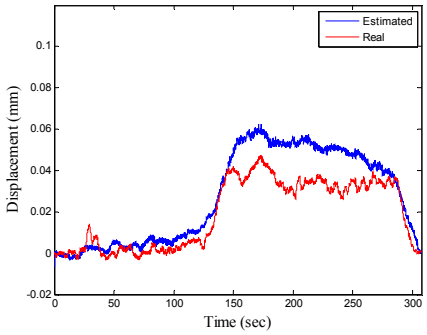

(a) Intact Case— First try

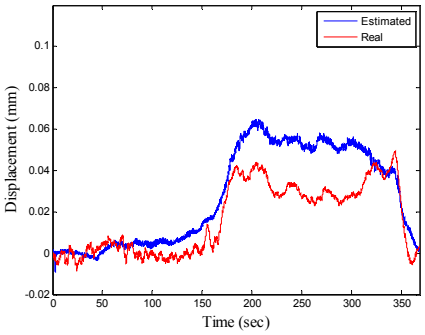

(b) Intact Case—Second try

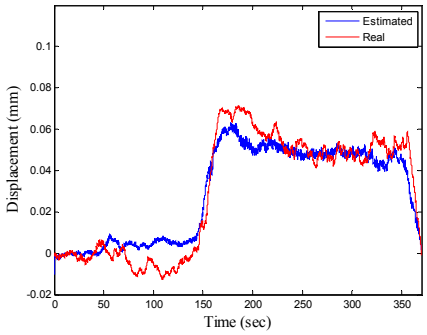

(c) Damage Case 1— First try

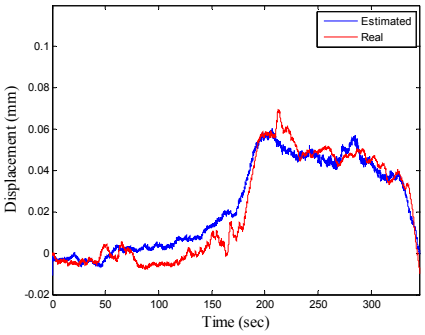

(d) Damage Case 1— Second try

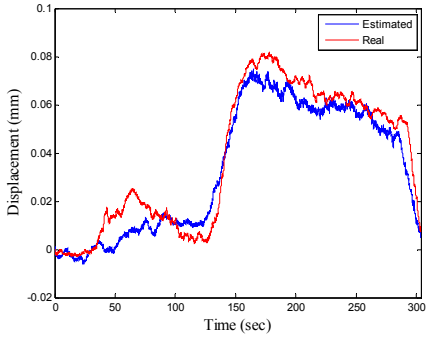

(e) Damage Case 2— First try

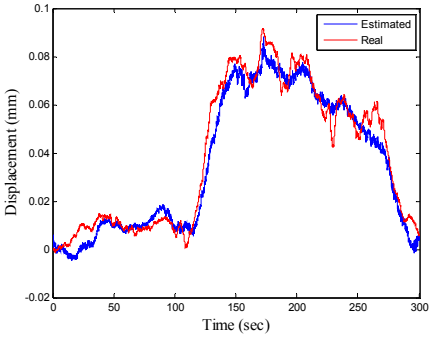

(f) Damage Case 2— Second try

Fig. 12 Results of the third lab-scale experiment to estimate displacement at the top of the lab-scale test structure

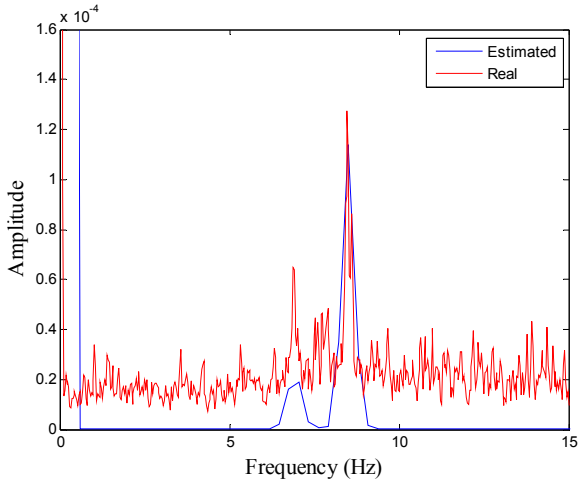

Fig. 13 PSD data for real and estimated displacement of Damage Case 2— First try

To successfully perform experiments to measure the real displacement, we needed to find a method to accurately measure and fabricate the new structure having smaller stiffness, inducing large displacement, due to the fixed current velocity. Figs. 12 and 13 show the accuracy of the multimetric displacement estimation for quasi-static displacement and dynamic displacement, respectively. Therefore, this method was determined to be valid.

4. Verification of the experiment using numerical simulation

4.1 Outline of the numerical simulation

ABAQUS (ABAQUS 6.10.1, 2010), a commercial FE analysis code, was used to calculate the natural frequencies for verification of the experimental results. Figs. 14(b) and 14(d) show the entire shape and the bottom shape of the elaborately simulated lab-scale test structure, respectively. As for the upper part of the lab-scale test structure, instead of simulating accelerometers, the weight of these was added to the upper part in modeling. Added mass was applied on the submerged part of the lab-scale test structure in the simulations to represent the water level increases in the experiment. The intact condition was simulated as shown in Fig. 14(d), where all bolts were fixed at four locations, satisfying a constraint condition in the longitudinal, fore-and-aft, and side-to-side directions. Damage Cases 1 and 2 were simulated by removing the constraint condition at the locations where the bolts are removed. The number of nodes and elements are 6,812 and 3,916, respectively, and the element type is a hexahedral solid. Because modal analysis for natural frequencies is theoretically not influenced by external forces, the effects of current velocity changes cannot be considered in the ABAQUS modeling.

(a) Entire model—real

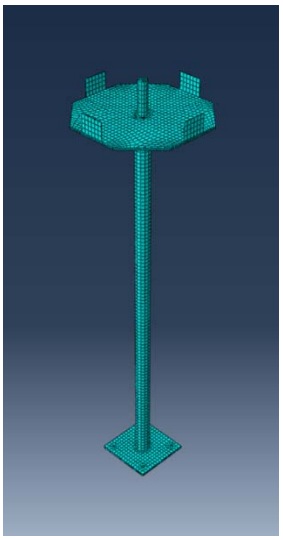

(b) Entire model—simulated

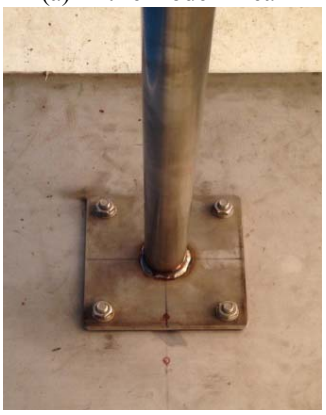

(c) Boundary condition—real

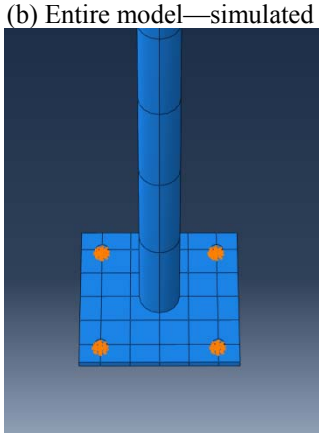

(d) Boundary condition—simulated

Fig. 14 Real and simulated numerical model of the lab-scale test structures

4.2 Added mass effect

As shown in Fig. 15, the experimental value of the first modal frequency in the fore-and-aft direction decreased by 0.6% from 8.61 to 8.56 Hz, while the numerical value decreased by 1.28%—more than double the experimental value from 8.59 to 8.48 Hz. However, in the case of the second bending mode in the fore-and-aft direction, the experimental and numerical values are very close to each other. Therefore, it can be confirmed that the previous equation for added mass—Eq. (2)—is correct for the second bending mode. However, in the case of the first bending mode, the particular constant is needed to fit the experimental and numerical values. This indicates that the added mass coefficient is dependent on each mode (i.e., frequency).We could find the correct added mass coefficient in the first bending mode by model updating.

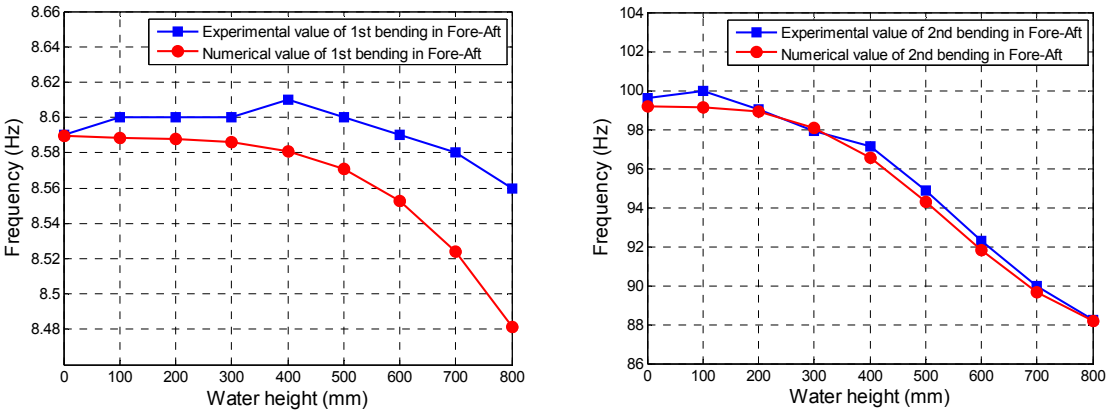

(a) First bending modal frequency (b) Second bending modal frequency

Fig. 15 Experimental and numerical values of the first and second frequency in the fore-and-aft directionas water level increase

5. Conclusions

The motivation behind this paper came from the long-term observation of the identified natural frequencies of the Uldolmok tidal current power plant (TCPP). The natural frequencies of this structure under severe current environments have changed with the M2 (approximately 12 hours) and M4 (approximately 6 hours) tidal constituents. To study the main factor responsible, two lab-scale experiments were carried out using the lab-scale monopile-type test structure, simplified for the Uldolmok TCPP structure. We observed changes of the first natural frequency by controlling the main factors, including the water level, current velocity, and degree of damage in the boundary connections. In the first lab-scale experiment, the natural frequencies were extracted through the eigensystem realization algorithm(ERA) method for the acceleration response under impact excitation. In the second lab-scale experiment, the natural frequencies were calculated by the peak-picking method from the power spectral density (PSD) data. In addition, for the same purpose of SHM with the previous two experiments, another lab-scale experiment was conducted to verify the displacement estimation proposed by Park *et al*. (2013) using data fusion, and the degree of damage could be shown by damage index (β), the normalized damage factor (NDF), which is from a scaling coefficient α. Our concluding remarks are as follows:

- Offshore structures consisting of cylinder members can be affected by added mass, defined as Eq. (1). As shown in Fig. 15, however, this is not always applied on all modes; Eq. (1) is almost exact in the second bending mode; however, as for the first bending mode, the experimental decrease in the natural frequency was 46.9% of the numerical value. In other words, the added mass coefficient is dependent on the natural modes (i.e., frequency). Therefore, in monitoring vibration characteristics and assessing integrity of offshore structures, added mass effect should be accurately determined because natural frequency is the most fundamental factor in structural identification.

- Second lab-scale experiment indicated that the decrease of the natural frequencies depends on the degree of damage in the boundary connections under increase in current velocity. In the Intact Case and Damage Case 1 (degree of damage is not severe), there were slight changes in the natural frequencies; however, Damage Case 2 (degree of damage is severe) shows that stiffness decreases and nonlinearity increases as the degree of damage in the boundary connections becomes severe. In addition, in this situation, the natural frequencies decrease considerably as the current velocity increases. These results indicate that the degree of damage is an important component to influence the increase in nonlinearity and the dynamic characteristics of the structure.
- In the third lab-scale experiment, there were problems with accurately measuring the real displacement due to vibration from the pump and trouble with the installation of the LASER displacement meter with high accuracy. To accurately verify the estimated displacement, a measuring method for real (reference) displacement should be found. Nevertheless, the multimetric data fusion method proposed by Park *et al*. (2013) has sufficient validity in an intact and damaged cantilever beam. The error in Intact Case was large because of too small amount of displacement; however, it can be recognized that the error in Damage Case 2, which has the largest displacement, decreased through the comparison of Err_1andErr_2 of each boundary condition.
- We introduced damage index β in this study and compared Damage Cases 1 and 2 using this index. The degree of damage between the damage cases can be observed. The mean value of β in Damage Cases 1 and 2 were 4.44 and 6.51, respectively. This denotes the degree of damage.

Acknowledgments

This research was a part of the project titled “Development of active-controlled tidal stream generation technology” funded by the Ministry of Oceans and Fisheries, Korea (20110171) and KIOST research program (PE99322). The authors would like to express their appreciation for the financial support.

References

Celibi, M. (2000), “GPS in dynamic monitoring of long-period structures”, *Soil Dyn. Earthq. Eng.*, **20**(5), 477-483.

Cho, S.J., Sim, S.H., Park, J.W. and Lee, J.H. (2014), “Extension of indirect displacement estimation method using acceleration and strain to various types of beam structures”, *Smart Struct. Syst.*, **14**(4), 699-718.

Dassault Systemes Simulia Corp. (2010), *Abaqus/CAE user’s manual*, Version 6.10, Rhode Island, USA. http://baribal.cyf-kr.edu.pl:2080/v6.10/index.html.

DNV (2010), *Environmental Conditions and Environmental Loads*. Recommended Practice DNV-RP-C205, October 2010.

Fraenkel, P.L. (2007), “Marine current turbines: pioneering the development of marine kinetic energy converters”, *J. Power Energy*, **221**(2), 159-169.

Hallam, M.G., Heaf, N.J. and Wootton, L.R. (1977), *Dynamics of Marine Structures: Methods of Calculating the Dynamic Response of Fixed Structures Subject to Wave and Current Action*. (1st Ed.), CIRIA Underwater Engineering Group, London.

Han, S.H., Park, J.S., Lee, K.S., Park, W.S. and Yi, J.H. (2013), "Evaluation of vertical axis turbine characteristics for tidal current power plant based on in situ experiment", *Ocean Eng.*, **65**, 83-89.

HBM, MGCPlus operating manual. Available online: http://www.hbmdoc.com/fileadmin/mediapool/hbmdoc/technical/b0534.pdf (accessed on 14 Jan. 2014)

Huynh, T.C., Lee, S.Y., Kim, J.T., Park, W.S. and Han, S.H. (2013), "Simplified planar model for damage estimation of interlocked caisson system", *Smart Struct. Syst.*, **12**(3-4), 441-463.

Juang, J.N., and Pappa, R.S. (1985), "An eigensystem realization algorithm for modal parameter identification and model reduction", *J. Guid. Control Dynam.*, **8**(5), 620-627.

Kim, J.T. and Stubbs, N. (1995), "Damage detection in offshore jacket structures from limited modal information", *Int. J. Offshore Polar*, **5**(1), 58-66.

Lee, H.S., Hong, Y.H. and Park, H.W. (2010),"Design of an FIR filter for the displacement reconstruction using measured acceleration in low-frequency dominant structures", *Int. J. Numer. Meth. Eng.*, **82**(4), 403-434.

Lee, S.Y., Nguyen, K.D., Huynh, T.C., Kim, J.T., Yi, J.H. and Han, S.H. (2012), "Vibration-based damage monitoring of harbor caisson structure with damaged foundation-structures interface", *Smart Struct. Syst.*, **10**(6), 517–546.

Lee, S.Y., Huynh, T.C., Kim, J.T., Yoon, H.S. and H, S.H. (2013), "Vibration Characteristics of Gravity-Type Caisson Breakwater Structure with Water-Level Variation", *Int. J. Distrib. Sens. N.*, **2013**.

Li, H.N., Yi, T.H., Ren, L., Li, D.S., Huo, L.S. (2014), "Reviews on innovations and applications in structural health monitoring for infrastructures", *Struct. Monit. Maintenance*, **1**(1), 1-45.

Park, J.W., Sim, S.H., Jung, H.J. (2013),"Displacement estimation using multimetric data fusion", *IEEE/ASME T. Mechatronics*, **18**(6), 1675-1682.

Park, J.W., Sim, S.H., Yi, J.H. and Jung, H.J. (2014), "Numerical study of temperature-robust damage factor based on combination of an accelerometer and an inclinometer for a cantilever beam-type structure", *Frontiers of Structural and Civil Engineering*, accepted.

Salawu, O.S. (1997), "Detection of structural damage through changes in frequency: A review", *Eng. Struct.*, **19**, 718-723.

Sedlar, D., Lozina, Z. and Vucina, D. (2011), "Experimental investigation of the added mass of the cantilever beam partially submerged in water", *Technical Gazette*, **18**(4), 589-594.

Weiner, E.O., Julyk, J.L. and Rezvani, M.A. (1994), *Hydrodynamically Induced Loads on Components Submerged in High-level Waste Storage Tanks*, Report of US Department of Energy.

Yi, J.H., Kim, J.H., Jeong, W.M. and Chae, J.W. (2013c), "Field evaluation of optical-based three-dimensional dynamic motion measurement system with multiple targets for a floating structure", *Ocean Eng.*, **62**, 140-151.

Yi, J.H., Oh, S.H., Park, J.S., Lee, K.S. and Lee, S.Y. (2013a), "Flow-Turbine Interaction CFD Analysis for Performance Evaluation of Vertical Axis Tidal Current Turbines(I)", *J. Ocean Eng. Technol.*, **27**(3), 67-72.

Yi, J.H., Park, J.S., Han, S.H. and Lee, K.S. (2013b), "Modal identification of a jacket-type offshore structure using dynamic tilt responses and investigation of tidal effects on modal properties", *Eng. Struct.*, **49**, 767-781.

Yi, J.H., Park, J.S., Park, J.S. and Lee, K.S. (2012), "Long-term measurement of static strains of jacket type offshore structure under severe tidal current environments", *Korean Society of Civil Engineers*, **32**(6), 389-398.

Yi, J.H., Yun, C.B.(2004),"Comparative study on modal identification methods using output-only information", *Struct. Eng. Mech.*, **17**(3-4), 445-466.